Compression-shear-induced tilt azimuthal orientation of amphiphilic monolayers at the air-water interface: A $C_\infty \rightarrow C_{2v}$ transition in the flow of a two-dimensional hexatic structure

Mitsumasa Iwamoto,[1] Atsushi Tojima,[1] Takaaki Manaka,[1] and Ou-Yang Zhong-can[2]
[1]*Department of Physical Electronics, Tokyo Institute of Technology, 2-12-1, O-okayama, Meguro-ku, Tokyo 152-8552, Japan*
[2]*Institute of Theoretical Physics, The Chinese Academy of Sciences, P.O. Box 2735, Beijing 100080, China*
(Received 20 September 2002; published 21 April 2003)

Compression-shear-induced tilt azimuthal orientation of amphiphilic monolayer in tilting phases (L_2 and L_2') at the air-water interface is analyzed as dynamical equilibrium of the elastic distortion of orthogonally hexagonal structure of the molecules under compression-induced shear flow. It is shown theoretically that the compression can induce molecular tilts lying along and/or against the flow direction. All these tilts makeup the initial random tilt azimuth of the molecular tails along a uniform direction. At a threshold compression speed, it causes a $C_\infty \rightarrow C_{2v}$-symmetry transition at the air-water interface. With Maxwell displacement current and optical second-harmonic generation measurements, the above theoretical results are verified experimentally in a monolayer of 4-heptyloxy-4′-cyanobiphenyl.

DOI: 10.1103/PhysRevE.67.041711 PACS number(s): 64.70.Md, 68.15.+e

I. INTRODUCTION

Monolayers of amphiphilic molecules on a water surface exhibit very interesting behaviors as two-dimensional systems, and the physicochemical property of these monolyers has become a research topic in physics, chemistry, and biology since the discovery of the technique for the formation of floating monolayers by Langmuir [1]. With surface pressure-area (Π-A) measurement, the rich polymorphism and the phase transitions in monolayers of amphiphilic molecules have been recognized from the existence of kinks or plateaus in their Π-A isotherms. Recently, a variety of experimental techniques coupled with Π-A isotherm measurement have been developed for exploring the structure of monolayers. The equilibrium properties of insoluble monolayers at the air-water interface have been studied intensively, and many structures of monolayer phases have been elucidated. In a review paper by Kaganer *et al.*, the phase diagrams of fatty acid monolayers obtained from x-ray diffraction method and other approaches have been summarized with their Π-A isotherms [2]. Among the recognized phases, liquid condensed phases L_2 and L_2' are particularly interesting because they happen at the meeting point of two- and three-dimensional (2D, 3D) systems as well as in solid and liquid crystal (LC) phases: In both L_2 and L_2' phases, the polar heads of amphiphilic molecules form a distorted hexatic lattice in a manner as predicted by the theory [3] and shown schematically in Fig. 1. The long molecular axes of molecules in L_2 and L_2' phases are tilting toward a nearest neighbor (NN) if $\phi=0$ [Fig. 1(a)], and to a next nearest neighbor (NNN) if $\phi=\pi/2$ [see Fig. 1(b)], i.e., the stretching direction of the hexatic lattice as revealed lately in x-ray diffraction [4]. Here, one must understand that even though the tilt $\phi=\pi/2$ has not happened, $\phi=\pi/6$ is a potential NNN direction (Fig. 1). However, once tilt happens, the distorted hexatic lattice has only rectangle symmetry. Only two states of $\phi=\pi/2$ for NNN phase, and $\phi=0$ for NN phase remain even when the monolayer enters the solid phase ($\theta=0$) are probable as confirmed in x-ray experiment [4]. Very recently, the tilting phase transition was studied as a distortion of the orthogonal hexagonal orientation of molecules by a competition among the entropy of both head position and molecular axes orientation distributions, Lenard-Jones potential, and the work done by surface and bulk pressures [5,6]. The theory predicts a physically reasoning phase portion in a phase diagram between tilting and untilting phases and shows quantitative agreement with the measurement in monolayers of C_{14}-C_{24} acids [7].

The discovery of 2D structure in L_2 and L_2' phases has attracted much attention to the classical study of the flow behavior of monolayers [1], especially in searching for the coupling between the flow and the structure and the orientation [8–12]. In the classical study of the flow in monolayers, a number of surface viscosity measurements have been employed, but the effects of flow on the underlying structure of the monolayers have been overlooked [1]. However, with the development of the direct observation techniques such as Brewster angle microscopy (BAM), x-ray diffraction, and other spectroscopic techniques, this situation has been completely improved. Using observation techniques, the coupling between an imposed flow and the structure of monolayers on the water surface can be searched. Fuller's group [8–10], using BAM observation, showed the existence of a strong coupling between external flow and the orientational order of the fatty acid monolayer. By studying the L_2, L_2', and S (solid) phases, they argued that the structure of the monolayers is annealed by a shear flow, but the nature of the coupling depends on the phases. That is, only L_2' and S phases experience flow-induced reorientation in the lattice. In more detail, induced reorientation is accompanied by an appearance of shear bands in the monolayer at an angle of 45° to the flow axis. It was also revealed that sufficient extensional flow can induce a tilt azimuth aligned perpendicular to the extensional axis. With similar observation technique, Schwartz's group [11,12] revealed such shear-induced orientations in the O_v phase (similar to L_2' with NNN-azimuthal tilt) in docosanoic acid monolayers and found a shear-induced molecular precession [11], i.e., a flow-induced

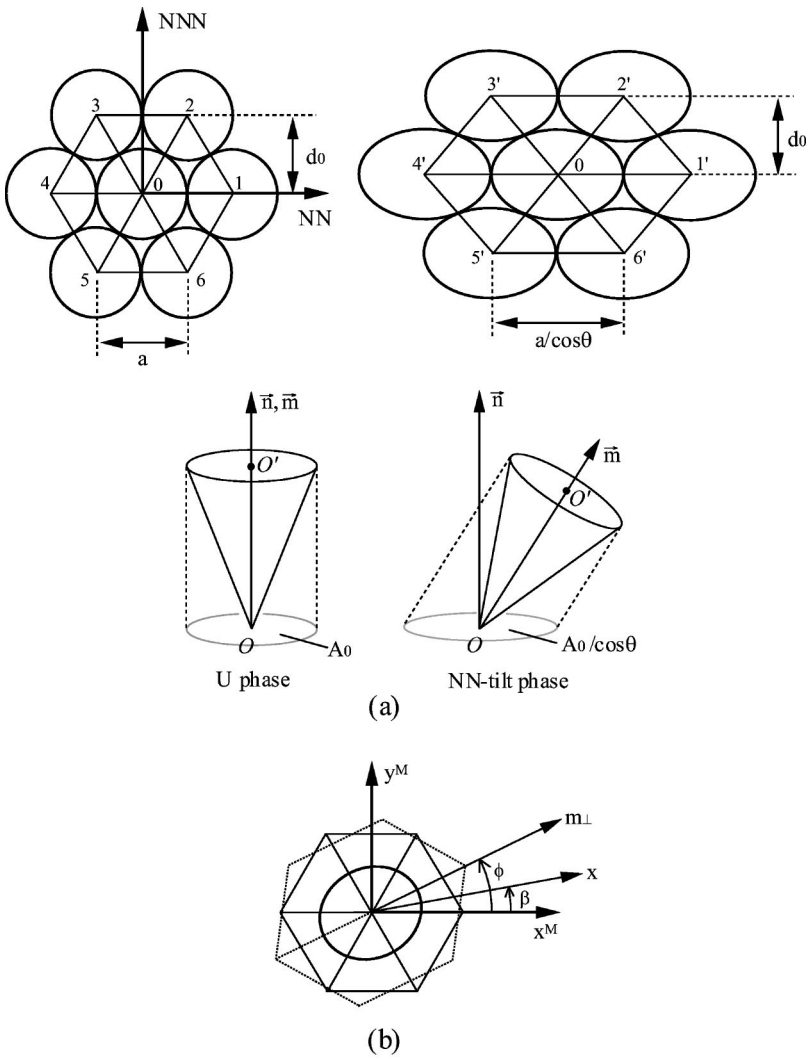

FIG. 1. (a) Model structure for untilted orthorhombic phase and its distortion towards a nearest neighbor (NN) regarded as L_2 phase. The structure of L_2' phase is tilted to the next nearest neighbor (NNN) and has been omitted in the figure. (b) The geometry for a random tilting domain, where $\vec{x}$ is the compression direction of the monolayer, ($\vec{x}^M$, $\vec{y}^M$) is one set of (NN, NNN)-tilting directions, and $\vec{m}_\perp$ denoted its tilt azimuthal direction.

alignment of alkyl chains. They then argued that the change in the monolayer structure is consistent with an alignment of the degenerate symmetry lines of the underlying molecular lattice with the flow, and the nature of the alignment is quite different from what is observed in nematic liquid crystals.

The shear-induced orientation is well known in bulk LC [13] and can be described by Ericksen-Leslie (EL) theory [14]. However, our understanding on the shear-induced orientation in monolayers is limited: EL theory deals only with flow-orientation coupling in nematic LC in which molecules possess orientation (director) ordering. So far there is no accepted model of hexatic flow that couples with shear-induced orientations. How to extend EL theory to the flow of monolayers with 2D hexatic ordering becomes an urgent challenge.

As a first step, let us study a compression-shear-induced tilt azimuthal orientation (CSTAO) in both L_2 and L_2' (including O_v) phases in a monolayer on the water surface. The important and fundamental approach of our study is that: by viewing the tilt C_6 axis of the hexatic lattice as LC director $\vec{m}$ in an EL-hydrodynamic (or viscous) stress tensor [14], the CSTAO is described as a dynamic equilibrium between the hydrodynamic and the static (or elastic) stresses given by the tilt distortion of the orthogonal hexagonal monolayer structures. The derived dynamic equation of CSTAO shows a threshold of the compression speed of the molecular area V_{AC}^*, below (above) which the initial random tilt distortion of azimuth of the long tails of molecules rotates continuously in a direction along or against (normal) the flow, and causes a $C_\infty \rightarrow C_{2v}$-symmetry transition in a monolayer at the air-water interface. Furthermore, this effect is clearly detected in a monolayer of 4-heptyloxy-4′-cyanobiphenyl (7OCB) by Maxwell displacement current (MDC) [15] and optical second-harmonic generation (SHG) [16] measurement techniques. These techniques allow us to detect spontaneous and nonlinear polarization of monolayers that appear to be phase dependent.

The arrangement of this paper is as follows. In Sec. II, we

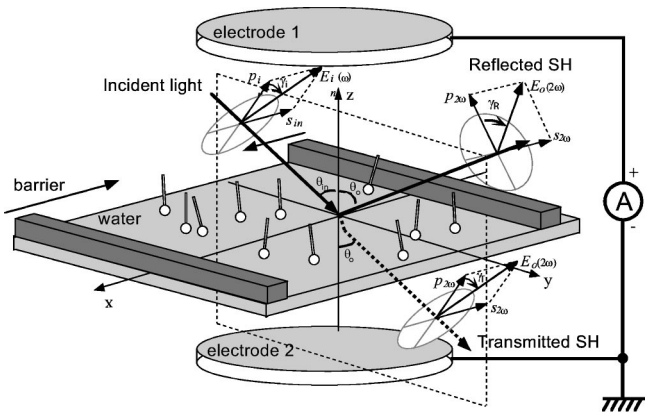

FIG. 2. Experimental setup for MDC and SHG measurement. The monolayer is described as the $z=0$ plane and two moving barriers are described as the two lines $x=\pm x_0$ on the plane at $t=0$.

describe how to use the MDC-SHG spectroscopy method to detect both the usual 2D-phase transition and the flow-induced transition by compression of a monolayer and its detailed implementation in a 7OCB monolayer. In Sec. III, we build a continuum theory for the 2D monolayer with tilting-hexatic symmetry. The main task is devoted to derive the elastic stress tensor of distortion in the orthogonal hexagonal orientation and the number of elastic constants, taking into account of the C_6-tilting symmetry. In particular, the EL theory and the viscous tensor for 3D LC are reformed into a 2D representation to solve the monolayer flow-orientation problem. In Sec. IV, the solution of compression-shear-induced tilt azimuth orientation is extensively discussed in comparison with our experimental finding in the 7OCB monolayer as well as those observed by Fuller's group [8–10] and Schwartz's group [11,12]. Section V gives the conclusion.

II. DETECTION OF $C_\infty \rightarrow C_{2v}$ TRANSITION BY MDC-SHG MEASUREMENT

Different from the BAM observation and the x-ray diffraction technique, MDC-SHG spectroscopy can provide the information on time dependent and continuous phase transition process in a monolayer under compression. As its name implies, the measurement setup is composed of two systems, one MDC measurement system and a SHG measurement system. In this section, the two systems as well as the principle and the method for detecting phase transition in monolayers are summarized. The detailed geometric and physical parameters for the whole system are given in Sec. IV.

Figure 2 shows a schematic diagram of our composed MDC-SHG measurement system that is attached to a Langmuir trough: A two-electrode arrangement (electrode area 45.4 cm^2) is used to measure MDC in short circuit and a *Q*-switched Nd:YAG (yttrium aluminum garnet) laser (Big Sky Laser Tech. Inc., maximum power 50 mJ, wavelength 1.064 μm, pulse duration <7 ns, pulse rate <20 Hz, laser beam spot size 28 mm^2) is used as a source of fundamental wave for SHG measurement. Briefly, in the MDC measurement, electrode 1 is suspended in air and is placed parallel to the water surface at a distance of 1 mm from the water surface. Electrode 2 is a golden spiral immersed in water. The two electrodes are connected through an electrometer. Due to the spontaneous polarization P_z of the monolayer charge Q_1 is induced on electrode 1, where

$$Q_1 = -\frac{P_z B}{L} - C\phi_s . \tag{1}$$

Here B is the working area of electrode 1, C is the capacitance between electrode 1 and the water surface, L is the distance between electrode 1 and the water surface, and ϕ_s is the surface potential of water.

The induced charge Q_1 changes in accordance with the orientational motion of the polar molecules on the water surface and the change of surface density of molecules by monolayer compression. This change of charge generates transient current and is recorded as MDC. P_z is expressed as $P_z = P_0 \vec{n}\cdot\vec{m}$, where $\vec{n}$ is a unit vector in the z direction, which is normal to the water surface [see Fig. 1(a) and Fig. 2]. P_0 is the spontaneous polarization and is a function of the order parameter in the dipolar orientation around the director $\vec{m}$. As P_z changes along with the orientational motion around P_0 and the director $\vec{m}$, the structural change in monolayers accompanying the orientational change of the z component can be detected by MDC measurement. The detailed formulas for calculation of P_0 from MDC can be found in Refs. [17,18].

Similarly, as the monolayer symmetry is broken at the interface, nonlinear polarization arising from quantum interaction between electrons in the molecules and the external electric field is induced in monolayers by laser irradiation. Second harmonics (SH) is thus generated from monolayers at the water surface. The induced nonlinear polarization $\vec{P}^N$ depends on the monolayer structure. For example, for monolayer with uniaxial C_∞ symmetry that orients its director in the $\vec{m}$ direction, $\vec{P}^N$ is expressed as [16]

$$\vec{P}^N = s_{14}(\vec{E}\cdot\vec{m})(\vec{E}\times\vec{m}) + [(s_{33}-s_{15}-s_{31})(\vec{E}\cdot\vec{m})^2 + s_{31}\vec{E}^2]\vec{m} + s_{15}(\vec{E}\cdot\vec{m})\vec{E}, \tag{2}$$

where $\vec{E}$ is the electric field of the source wave and s_{ij} being functions of the order parameters in the molecular orientation around the director $\vec{m}$ are the components of second-order susceptibility (SOS) tensor of monolayers. Since $\vec{P}^N$ varies with the monolayer structure, the structural change can be detected sensitively by SHG. For the SHG measurement, the optical arrangement is also shown in the Fig. 2, where θ_{in} and θ_o are the incident and the output angles, respectively. With polarizers (P_1, P_2, P_3), s and p waves of incident fundamental light and output SH light are separated.

In the present MDC-SHG measurement, monolayers of 7OCB are compressed from both sides by moving two bar-

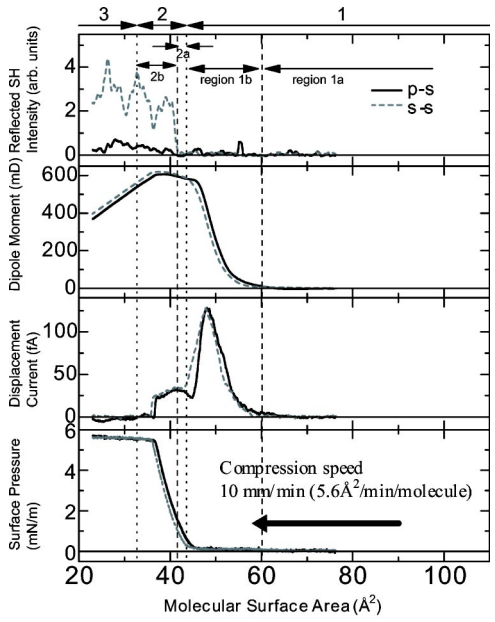

FIG. 3. A typical example for 7OCB monolayer for the measurement of MDC, SHG, and Π with change of molecular area *A*. From the change of Π-*A* the diagram can be distinguished as three regions as shown in the figure: 1 for $A>44$ Å^2, 2 for 36 Å$^2<A<44$ Å^2, and 3 for $A<36$ Å^2. However, with MDC-SHG measurement, regions 1 and 2 can be further divided as 1a for $A>60$ Å^2, 1b for 44 Å$^2<A<60$ Å^2, 2a for 41 Å$^2<A<44$ Å^2, and 2b for 36 Å$^2<A<41$ Å^2. The possible phase transitions in the corresponding regions are discussed in the text. The dashed lines are the measured results in the compression process different from that in measuring the solid lines. Both show a good repetition of the present experimental approach.

riers at a speed of $V_0=10$ mm/min along the *x* direction, and with a Wilhelmy plate, MDC-SHG signals together with the Π-*A* isotherm are recorded.

Figure 3 shows typical results of MDC-SHG measurement in a 7OCB monolayer, the surface pressure-molecular area diagram Π-*A* of 7OCB. From the surface pressure area isotherm, the molecular area is tentatively divided into three regions. The surface pressure is immeasurably low in the region of molecular surface area greater than 44 Å^2 (region 1), it gradually increases with a slope in the region of 36 Å$^2<A<44$ Å^2 (region 2), and finally it saturates at a surface pressure of 5.8 mN/m (region 3). But, judging from the characteristic behaviors of MDC and SHGs observed in regions 1 and 2, it is postulated that the monolayer undergoes a series of phase transitions $O_v\rightarrow L_2'\rightarrow L_2\rightarrow U$ (untilt phase) with increasing area compression. In more detail, at the beginning of the monolayer compression, MDC is very small, but nonzero, in the region greater than 60 Å^2 (region $1a$), whereas it is generated in the region between 44 Å^2 and 60 Å^2 (region $1b$). These results indicate that the monolayer which initially consists of rich mosaic domains with polarization in the *z* direction are gradually packed up by monolayer compression in the region 1. As MDC is generated from the change of induced charge Q_1 given by Eq. (1) in association with the orientational change of the molecules, MDC gives a peak in the vicinity of 50 Å^2, in the region earlier than that of the so-called $C_\infty\rightarrow C_{2v}$ transition to be discussed later. On the other hand, in the 41 Å$^2<A<44$ Å^2 region $2a$, the generation of SH is similar to that appeared in region 1, where *p*-*p* and *s*-*p* SH signals are generated (also reported in Fig. 1, Ref. [40], where MDC-SHG experiment using 532 nm wavelength laser beam is shown), whereas *p*-*s* and *s*-*s* SH signals are not generated. In contrast, MDC is nearly constant. This situation changes with further monolayer compression as shown in region $2b$, where a strong *s*-*s* SHG signal appears suddenly at the onset the 36 Å$^2<A<41$ Å^2 region $2b$, while the measured MDC shows a very smooth change. Sudden appearance of *p*-*s* SHG signal at the same point is also detected, though not very strong. These characteristic behaviors in SHG and MDCs indicate that rich mosaic domains appearing in region 1 and further in region $2a$, where the tilt azimuths are in random, though molecules are oriented in tilted hexatic structures in each domain, i.e., macroscopically the surface is still in C_∞ symmetry with the surface normal $\vec{n}$ as the C_∞ axis. However, such a situation is broken when $A<41$ Å^2, and in region $2b$, $C_\infty\rightarrow C_{2v}$ transition of the interface symmetry happens. Experimentally, we may consider that the amphiphilic layers remain as monolayers below the critical molecular surface area of 41 Å^2 because changes of surface pressure and MDC at this critical molecular area are smooth. If the layers lose the monolayer structure, both MDC and surface pressure should change abruptly. However, such changes are not seen in the figure. In the following, we focus our attention on this phase transition detected by SHG and MDC, and will discuss it in association with the CSTAO.

As mentioned earlier, nonlinear polarization $\vec{P}^N$ induced by laser irradiation can be expressed by Eq. (2) [16]. Originally, the derivation of this equation is based on the assumption that the macroscopic forms of the C_∞ orientation still holds for the present hexatic symmetry because the SOS tensor of C_6 symmetry is the same as that of C_∞ symmetry [19].

With Eq. (2) and of the geometry of the incident light as shown in Fig. 2, the expression of nonlinear polarization for generation of the reflected *s*-*s* SHG wave from each domain can be obtained as

$$P^N_{s-s}=\vec{P}^N\cdot\vec{s}=E_s^2[(s_{33}-s_{15}-s_{31})\sin^3\theta\cos^3\gamma + (s_{31}+s_{15})\sin\theta\cos\gamma]. \quad (3)$$

In the derivation of Eq. (3), it is assumed that $\vec{E}=E_s\vec{s}$ with $\vec{s}=(1,0,0)$ and $\vec{m}=(\sin\theta\cos\gamma,\sin\theta\sin\gamma,\cos\theta)$ as in Eq. (2). Here, θ is the tilt angle of C_6 axis $\vec{m}$ from the surface normal $\vec{n}$, and γ is the azimuthal angle of $\vec{m}$ from the compression direction **x** (see Fig. 2). In experiment, the generated SH depends on the laser radiated area, i.e., the average of P^N_{s-s} over domains in the laser irradiated area. This is the main contribution to the generation of SH. It is found that, obviously, $P^N_{s-s}\neq 0$ occurs only for $\langle\cos\gamma\rangle$ and $\langle\cos^3\gamma\rangle$ are nonvanishing, where $\langle\cdots\rangle$ denotes the average over domains in the laser irradiated area. Therefore, the appearance of *s*-*s* SHG signal reveals the tilt azimuth orientation either along or against the flow, i.e., the existence of a $C_\infty\rightarrow C_{2v}$

transition of the interface. Similarly, nonlinear polarization P^N_{p-s} for the generation of the *p-s* SHG can be calculated, and the sudden appearance of *p-s* SH signals at the transition point can be explained by the same $C_\infty \rightarrow C_{2v}$ transition, though it is not so clearly observed in Fig. 3. The different patterns of P^N_{p-s} and P^N_{s-s} can be understood from the expression of P^N_{p-s} in a domain as [16]

$$P^N_{p-s} = \vec{P}^N \cdot \vec{s} = E_p^2[(s_{33} - s_{15} - s_{31})(\sin\theta\cos\theta_{in}\sin\gamma + \cos\theta\sin\theta_{in})^2 + s_{31}]\sin\theta\cos\gamma. \quad (4)$$

Equation (4) is obtained from Eq. (2) by assuming that $\vec{E} = E_p \vec{p}_{in}$ with $\vec{p}_{in} = (0, \cos\theta_{in}, \sin\theta_{in})$, where θ_{in} is the incident angle as defined above. Equation (4) reveals again that $P^N_{p-s} \neq 0$ happens only when $\langle\cos\gamma\rangle$, $\langle\cos^3\gamma\rangle$, and $\langle\sin\gamma\cos\gamma\rangle$ are nonvanishing. This is different from P^N_{s-s}. The expression is more involved and depends on more parameters, such as θ_{in}, etc. Therefore, as a signal to detect the phase transition in a monolayer, P^N_{s-s} is more sensitive and not be screened by the incident geometry. The reflected intensity of *p-s* is obviously lower than that of *s-s* as shown in Fig. 3 and may be due to the scratching off by the incident geometry.

According to the mentioned analysis, one can conclude that the SHG measurement shown in Fig. 3 does reveal a compression-shear-induced tilted azimuth orientation: A $C_\infty \rightarrow C_{2v}$ transition occurs in the 7OCB monolayer. Furthermore, this transition is also confirmed by the smooth change of MDC observed at the onset of this transition in region $2b$: MDC reveals the phase transition accompanying the change of the *z* component of the molecular dipole change and must be independent of the azimuthal orientation change [see Eq. (1)].

III. THE GENERALIZED EL THEORY

In order to understand the compression-induced orientation transition, it is necssesary to analyze the 2D flow and its effect on the orientation. The fluid dynamical property of monolayer is still a difficult subject [20]. In both classical analysis [21,22] and modern studies [11,12,23–28], the monolayer flow is modeled as a flow resistance with a 2D surface viscosity $\mu_s = \mu_m h$, where μ_m is the equivalent 3D bulk shear viscosity and h is the layer thickness (see, for example, Ref. [26]). Obviously, such a treatment does not satisfy the present case where the monolayer is in the L_2 or L_2' phase with tilting-hexatic symmetry. Especially, for the discussion of the effect of flow-induced tilt azimuth orientation, such as experiments by Fuller and Schwartz's groups [8–12] as well as our observation in the 7OCB monolayer described in Sec. II, the anisotropy of the coupling between flow and tilting must be taken into account. The first successful treatment of an anisotropic flow was the dynamical theory of nematic LC (NLC) developed by Ericksen [29] and Leslie [30]. As mentioned in Sec. I, the EL theory of LC allows for anisotropic coupling between the flow and the orientation of the LC director $\vec{m}$ (in the present study, $\vec{m}$ refers to the tilting direction of L_2 or L_2' monolayer) but takes no account of the hexagonal lattice structure of the monolayer in L_2 and L_2' phases. Therefore, in the following two sections, a brief description of the EL theory and an extension to make it to satisfy the lattice structures are given. In sequent subsections, the extended EL theory is used to analyze the discussed problems.

A. EL theory

Assuming incompressible LC fluid, the usual Ericksen-Leslie continuum theory for 3D bulk LC can be expressed by the following two dynamical equations [14]:

$$\rho\frac{d\vec{v}}{dt} = \vec{f} + \vec{\nabla}\cdot\vec{\vec{t}}, \quad (5)$$

$$I\frac{d^2}{dt^2}\vec{m} = \vec{G} + \vec{g} + \vec{\nabla}\cdot\vec{\vec{\pi}}, \quad (6)$$

where ρ is the density of the LC (assumed to be constant), I is the density of inertia moment associated with the rotation of the director $\vec{m}$, $\vec{v}$ is the velocity field, $\vec{f}$ is the density of body force, $\vec{\vec{t}}$ is the stress tensor, and $\vec{G}$ is the director body force induced by external fields (such as the electric field used in LC display device), while $\vec{g}$ as well as $\vec{\vec{\pi}}$ are the body force and the surface stress of director, respectively, relating to the Ossen-Zöcher-Frank-free energy F [31]. In details, the free energy F, the most important formula in LC, serves to describe the elastic energy for deformed director pattern and can be written as

$$F = \frac{1}{2}k_{11}(\vec{\nabla}\cdot\vec{m})^2 + \frac{1}{2}k_{22}(\vec{m}\cdot\vec{\nabla}\times\vec{m} - k_2)^2 + \frac{1}{2}k_{33}(\vec{m}\times\vec{\nabla}\times\vec{m})^2, \quad (7)$$

where k_{11}, k_{22}, k_{33}, and k_2 are Frank-elastic constants, among which k_2 describes the chirality of the LC: $k_2 > 0$ for right handed cholesteric LC (chLC) and $k_2 < 0$ for left handed chLC, and $k_2 = 0$ for achiral NLC. Thus,

$$\vec{g} = \gamma\vec{m} - \vec{\beta}\cdot\vec{\nabla}\vec{m} - \partial F/\partial\vec{m} + (\mu_2 - \mu_3)\vec{M} + (\mu_5 - \mu_6)\vec{m}\cdot\vec{\vec{d}}, \quad (8)$$

$$\vec{\vec{\pi}} = \vec{\beta}\vec{m} + \partial F/\partial(\vec{\nabla}\vec{m}), \quad (9)$$

where μ_i, $\vec{M}$, and $\vec{\vec{d}}$ will be described later in details. γ and $\vec{\beta}$ are arbitrary scale and vector constants, and they can be determined by given boundary conditions and the relation $\vec{m}\cdot\vec{m} = 1$.

Equation (5) corresponds to the generalized Navier-Stokes equation, while Eq. (6) specifies the coupling between the flow and the director rotation.

For the present investigation, the most important quantity is the stress tensor $\vec{t}$ which can be separated into a static (i.e., elastic) part and a hydrodynamic (i.e., viscous) part as

$$t_{ij}=t_{ij}^{0}+t_{ij}', \tag{10}$$

where

$$t_{ij}^{0}=-p\,\delta_{ij}-\frac{\partial F}{\partial m_{k,i}}m_{k,j}, \tag{11}$$

$$t_{ij}'=\mu_1 m_k m_n d_{kn} m_i m_j+\mu_2 m_i M_j+\mu_3 m_j M_i+\mu_4 d_{ij} +\mu_5 m_i m_k d_{kj}+\mu_6 m_j m_k d_{ki}. \tag{12}$$

In Eqs. (10)–(12), p is the bulk pressure, $\mu_1-\mu_6$ are the coefficients of viscosity, named Leslie coefficients, and d_{ij} and w_{ij} are the symmetric and asymmetric part of $\vec{\nabla}\vec{v}$, respectively,

$$v_{ij}=d_{ij}+w_{ij}, \tag{13}$$

$$d_{ij}=\frac{1}{2}(v_{i,j}+v_{j,i}), \tag{14}$$

$$w_{ij}=\frac{1}{2}(v_{i,j}-v_{j,i}). \tag{15}$$

From Eq. (15), the vector $\vec{M}$ in Eq. (8) is defined as

$$\vec{M}=\frac{d}{dt}\vec{m}-\vec{\vec{w}}\cdot\vec{m}. \tag{16}$$

With these, the equations of the EL theory are complete.

B. Fluid field of CSTAO

The generalization of the EL theory to deal with the CSTAO problem requires two steps: (1) A straightforward derivation for the change of 3D quantities and 3D equations into their corresponding 2D forms; (2) Reconstruction of the quantities and formulas to fulfill the novel symmetry and structures. As a first example, we consider the velocity field. In Sec. III A, we have assumed $\rho=$const for 3D LC. The corresponding equation of conservation of mass is given by

$$\frac{\partial}{\partial t}\rho+\vec{\nabla}\cdot(\rho\vec{v})=0. \tag{17}$$

However, in the case of CSTAO the monolayer cannot be assumed as incompressible, i.e., $\rho\neq$const, apparently, it has a 2D-density form

$$\rho=\frac{Nm_0}{2X_0(t)L}, \tag{18}$$

where N is the total number of molecules in the monolayer, m_0 is the molecular mass, $2X_0(t)$ is the distance between two barriers at time t, and L is the width of the Langmuir trough along the y direction [Fig. 2(b)]. Substitution of ρ into Eq. (17) gives the velocity field

$$\vec{v}(x,t)=\left(\frac{V_0 x}{V_0 t-x_0},0\right)=(v_x,v_y), \tag{19}$$

where V_0 is the speed of the barriers mentioned earlier in Sec. II and $\pm x_0$ (with $x_0>0$) are the initial positions of the two barriers from the central position ($x=0$) of the rectangular shaped Langmuir trough at time $t=0$. To focus our attention on the orientation mechanism, we consider the case in which the velocity of the monolayer is dominant, where the coupling to the subphase (water) has been neglected as treated in Ref. [12]. From Eq. (19) one can prove that for uniform molecular area in the monolayer, the area at time t is given by

$$A(t)=A(0)(1-V_0 t/x_0), \tag{20}$$

that is, the compressed speed

$$V_{AC}=[A(0)-A(t)]/t=A(0)V_0/x_0 \tag{21}$$

is constant. In the present experiment on the 7OCB monolayer, $V_{AC}=5.6$ Å^2/min. The velocity field given in Eq. (19) has a nonvanishing compression shear

$$d_{11}=\partial v_x/\partial x=-V_{AC}/A(t). \tag{22}$$

Other tensor components, d_{ij} as well as w_{ij}, are zero [see Eqs. (14) and (15)]. Obviously, d_{11} increases as molecular area compression increases. This is the reason why CSTAO can happen in the L_2 and L_2' phases, the region 2 in Fig. 3.

The reconstruction of a 2D Frank-elastic energy is quite a task, though it can be carried out by a straight formed calculation from the 3D F [32,33]. Fortunately, the spatially uniform d_{11} and $A(t)$ shown in Eqs. (20) and (22) offer the possibility that the director field $\vec{m}$ can also be assumed to be spatially uniform in a domain. In other words, in the present study the detailed form of the 2D-Frank-free energy is temporally not involved. In the present special case, terms relating to F in Eqs. (8)–(11) are confined only to the elastic energy of the distorted hexatic-tilting F_e (see below for details). That is, one should note that the Frank energy F is only a part of the elastic energy to describe the deformation of the tilt director $\vec{m}$. In order to reform EL theory to fulfill the L_2 and L_2' phases, the elastic energy of the monolayers should include deformation energy of the hexatic lattice structure of the polar heads of molecules. Thus, the static stress tensor given in Eq. (11) has to be extended to involve the part induced by the lattice deformation as

$$t_{ij}^{0}=-\Pi_{ij}-\sigma_{ij}, \tag{23}$$

where the curvature stress has been discarded on account of the reasons mentioned earlier, Π_{ij} is the 2D surface stress to replace the original 3D bulk pressure $p\,\delta_{ij}$, and the novel stress tensor σ_{ij} represents the elastic stress tensor of the hexagonal lattice during the tilting process, i.e., we have referred the untilting phase [Fig. 1(a)] as the equilibrium lattice

state. One must note that in Eq. (23) the 2D Π_{ij} cannot be written as 2D surface pressure $\Pi\delta_{ij}$ because the considered domains are now in the tilting L_2 or L_2' phases and must be treated as anisotropic surface. With our experimental geometry, generally, we have $\Pi_{11}\neq\Pi_{22}$ and $\Pi_{12}=0$ [see Fig. 2(b)]. The reason for doing this can be clearly seen from Fig. 1: Tilting will induce stretching deformation of the hexagonal lattice. Calculation of the elastic energy of monolayers in L_2 and L_2' phases has been a recent subject for study [34]. In these studies, the L_2 and L_2' phases are treated as disordered solids and a general form of the free energy for tilted C_{6v} symmetry is established. It involves a set of order parameters where the coupling between the elastic 2D-lattice system of head groups and the rotational ordering of tails has been described in terms of microscopic translational-rotational coupling parameters. In other words, in their theory, the orientational and the 2D-lattice-order parameters are treated independently and relaxed in coupling. However, as commented in Ref. [35] by Sirota, in the condensed phases, where the long axes are like closely packed cylinders, tilting of the long axis will determine the distortion completely. This distortion happens in a way that causes the stretching of the projected lattice cell along the tilting direction with a ratio of $1/\cos\theta$, where θ is the tilting angle from the normal direction. For example, as illustrated in Fig. 1(a), on account of the stretching induced by tilting, the six NN positions indicated by 1, 2, 3, . . . , and 6 in untilting phase shift to the corresponding six positions indicated by $1'$, $2'$, $3'$, . . . , and $6'$ in the tilting phase. In other words, the position expressed as

$$\left(a\cos\left(\frac{n-1}{3}\pi-\phi\right),a\sin\left(\frac{n-1}{3}\pi-\phi\right),0\right)$$

$$(n=1,2,\ldots,6)$$

in xy coordinate with origin at (0, 0, 0) in the U-phase shifts to

$$\left(a\cos\left(\frac{n-1}{3}\pi-\phi\right)\Big/\cos\theta,a\sin\left(\frac{n-1}{3}\pi-\phi\right),0\right)$$

$$(n=1,2,\ldots,6)$$

in the t phase if tilting occurs in the NN or x direction, where $a=2d_0/\sqrt{3}$. As mentioned in Sec. I, Sirota's viewpoint has been used as an approach to calculate successfully the phase portion between U-t phase transition in the Π-A diagram [5,6]. In the following section, the same approach will be used to calculate the elastic stress tensor σ_{ij}.

C. Stress tensor σ_{ij}

Before going into practical calculation let us first trace back to the classical elastic mechanics of crystals [19,22]: The elastic energy of distorted crystal is written in a tensorial summation as

$$F_e=\frac{1}{2}c_{ijkl}\nu_{ij}\nu_{kl}, \tag{24}$$

where c_{ijkl} are the elastic constant tensors characterized by the symmetry of the crystal discussed in Ref. [19] and ν_{ij} is a finite strain tensor. According to solid mechanics [22], a finite strain is defined as follows: When a material point in the equilibrium position $\vec{a}$ ($\vec{r}^U$ in our case) is shifted to $\vec{x}$ ($\vec{r}^t$ in our discussion) as a result of deformation, the displacement is written as

$$\vec{u}=\vec{x}-\vec{a}. \tag{25}$$

Here $\vec{a}$ is the Eulerian coordinate of the material point and $\vec{x}$ is the Lagrangian one. The strain ν_{ij} is then defined by

$$dx_i dx_i-da_i da_i=2\nu_{ij}da_i da_j, \tag{26}$$

and can be found as

$$\nu_{ij}=\frac{1}{2}\left(\frac{\partial u_j}{\partial a_i}+\frac{\partial u_i}{\partial a_j}+\frac{\partial u_k}{\partial a_i}\frac{\partial u_k}{\partial a_j}\right). \tag{27}$$

If the third term in Eq. (27) is neglected, it becomes a linear relation with deformation and will be renamed as

$$s_{ij}=\frac{1}{2}\left(\frac{\partial u_j}{\partial x_i}+\frac{\partial u_i}{\partial x_j}\right). \tag{28}$$

On account of the tensor symmetry of $s_{ij}=s_{ji}$, Eq. (24) can be rewritten as the abbreviation form

$$F_e=\frac{1}{2}c_{\mu\nu}s_\mu s_\nu, \tag{29}$$

where the simpler matrix expression by index abbreviation is used in a manner as follows [19]: $C_{ijkl}\rightarrow c_{\mu\nu}$ by $(ij)\rightarrow\mu$ with $11\rightarrow1$, $22\rightarrow2$, $33\rightarrow3$, $23\rightarrow4$, $31\rightarrow5$ and $12\rightarrow6$, while $s_{ij}\rightarrow s_\mu$ for $i=j$ ($\mu=1-3$), and $2s_{ij}\rightarrow s_\mu$ for $i\neq j$ ($\mu=4-6$) with the same index abbreviation. Now let us turn to practical computation for the tilting deformation as shown in Fig. 1(b), where (x,y) is the laboratory coordinate system. x is in the compression direction of the monolayer as shown in Fig. 2, (x^M,y^M) is the frame fixed in the discussed domain with x^M direction parallel to NN one at u phase, $m_\perp$ is the tilt azimuthal direction for the discussed domain, and the tilted angle is θ. As the geometry shown in Fig. 1(b), we consider the six NN points of the origin at the water surface with their positions in the domain system at u-phase, stated in the preceding subsection, as

$$d\vec{a}^{M(1)}=\left(\frac{2}{\sqrt{3}}d_0,0,0\right),\quad d\vec{a}^{M(2)}=\left(\frac{d_0}{\sqrt{3}},d_0,0\right),$$

$$d\vec{a}^{M(3)}=\left(-\frac{d_0}{\sqrt{3}},d_0,0\right),\ldots. \tag{30}$$

We omit the terms $d\vec{a}^{M(n)}$ $(n=4,5,6)$. They can be obtained by

$$d\vec{a}^{M(n)}=\frac{2d_0}{\sqrt{3}}\left(\cos\left(\frac{n-1}{3}\pi\right),\sin\left(\frac{n-1}{3}\pi\right),0\right), \quad (31)$$

for $n=4$, 5, and 6. They are not in the calculation since they are symmetric with cases $n=1$, 2, and 3, respectively. In the tilting geometry given in Fig. 1(b), $d\vec{a}^{M(n)}$ changes to $d\vec{x}^{M(n)}$, terms already calculated in Ref. [5]. $|d\vec{x}^{M(n)}|^2$ can be obtained exactly as

$$|d\vec{x}^{M(n)}|^2=dx_i^{M(n)}dx_i^{M(n)}$$
$$=\left(\frac{2d_0}{\sqrt{3}\cos\theta}\right)^2\left[1-\sin^2\left(\frac{n-1}{3}\pi-\phi\right)\sin^2\theta\right]. \quad (32)$$

Substitution of Eqs. (30)–(32) into Eqs. (26)–(28) for $n=1$, 2, and 3, gives the following equations :

$$\left(\frac{2d_0}{\sqrt{3}\cos\theta}\right)^2[1-\sin^2\phi\sin^2\theta]-\left(\frac{2d_0}{\sqrt{3}}\right)^2=2s_{11}^M\left(\frac{2}{\sqrt{3}}d_0\right)^2, \quad (33)$$

$$\left(\frac{2d_0}{\sqrt{3}\cos\theta}\right)^2\left[1-\sin^2\left(\frac{\pi}{3}-\phi\right)\sin^2\theta\right]-\left(\frac{2d_0}{\sqrt{3}}\right)^2$$
$$=2s_{11}^M\left(\frac{d_0}{\sqrt{3}}\right)^2+4s_{12}^M\left(\frac{d_0^2}{\sqrt{3}}\right)+2s_{22}^Md_0^2, \quad (34)$$

$$\left(\frac{2d_0}{\sqrt{3}\cos\theta}\right)^2\left[1-\sin^2\left(\frac{2\pi}{3}-\phi\right)\sin^2\theta\right]-\left(\frac{2d_0}{\sqrt{3}}\right)^2$$
$$=2s_{11}^M\left(-\frac{d_0}{\sqrt{3}}\right)^2+4s_{12}^M\left(-\frac{d_0^2}{\sqrt{3}}\right)+2s_{22}^Md_0^2, \quad (35)$$

where $s_{\mu\nu}^M$ is the tilt-induced strain tensor in the domain frame. In fact, the calculation with the NN points of $n=4$, 5, and 6 gives the same equations, Eqs. (33)–(35). Solving Eqs. (33)–(35) lead to

$$s_{11}^M=\frac{1}{2}\tan^2\theta\cos^2\phi,$$

$$s_{12}^M=\frac{1}{2}\tan^2\theta\sin\phi\cos\phi, \quad (36)$$

$$s_{22}^M=\frac{1}{2}\tan^2\theta\sin^2\phi.$$

With the Sirota's approach, the tilting also causes a compression of the thickness of the monolayer, a change from h_0 at u phase to the $h_0\cos\theta$ at the t phase. Therefore, we have to extend the above calculation to take into account the deformation in the z dimension. The positions of the NN points at air-monolayer interface of the monolayer in the u phase are given by

$$d\vec{a}_{top}^{M(n)}=\left(\frac{2d_0}{\sqrt{3}}\cos\frac{n-1}{3}\pi,\frac{2d_0}{\sqrt{3}}\sin\frac{n-1}{3}\pi,h_0\right). \quad (37)$$

It can be rewitten as

$$d\vec{a}_{top}^{M(n)}=\overrightarrow{00'}+d\vec{a}^{M(n)}, \quad (38)$$

where $\overrightarrow{00'}$ is the position $(0,0,h_0)$ of the origin $0'$ on the top surface and $d\vec{a}^{M(n)}$ is defined at the bottom as shown in Eq. (31). After tilting, $d\vec{a}_{top}^{M(n)}$ is deformed into

$$d\vec{x}_{top}^{M(n)}=\overrightarrow{00'^t}+d\vec{x}^{M(n)} \quad (39)$$

where $\overrightarrow{00'^t}$ is the deformed position of $0'$ [Fig. 1(b)] and $d\vec{x}^{M(n)}$ is given by in Eq. (32). Thus, we have

$$|d\vec{a}_{top}^{M(n)}|^2=h_0^2+|d\vec{a}^{M(n)}|^2 \quad (40)$$

and

$$|d\vec{x}_{top}^{M(n)}|^2=h_0^2+2\overrightarrow{00'^t}\cdot d\vec{x}^{M(n)}+|d\vec{x}^{M(n)}|^2. \quad (41)$$

From the geometry shown in Fig. 1(b), we have

$$2\overrightarrow{00'^t}\cdot d\vec{x}^{M(1)}=\frac{4h_0d_0}{\sqrt{3}}\tan\theta\cos\phi, \quad (42)$$

$$2\overrightarrow{00'^t}\cdot d\vec{x}^{M(2)}=\frac{2h_0d_0}{\sqrt{3}}\tan\theta(\cos\phi+\sqrt{3}\sin\phi), \quad (43)$$

$$2\overrightarrow{00'^t}\cdot d\vec{x}^{M(3)}=\frac{2h_0d_0}{\sqrt{3}}\tan\theta(\sqrt{3}\sin\phi-\cos\phi). \quad (44)$$

Together with Eqs. (30) and (32), substitution of Eqs. (37), (40)–(44) into Eqs. (26) and (28), respectively, gives the novel equations for $n=1$, 2, 3 as

$$\frac{4h_0d_0}{\sqrt{3}}\tan\theta\cos\phi+\left(\frac{2d_0}{\sqrt{3}\cos\theta}\right)^2(1-\sin^2\phi\sin^2\theta)$$
$$-\left(\frac{2d_0}{\sqrt{3}}\right)^2=2s_{11}^M\left(\frac{2d_0}{\sqrt{3}}\right)^2+2s_{33}^Mh_0^2+4s_{13}^M\frac{2d_0h_0}{\sqrt{3}}, \quad (45)$$

$$\frac{2h_0d_0}{\sqrt{3}}\ \tan\theta(\cos\phi+\sqrt{3}\ \sin\phi)+\left(\frac{2d_0}{\sqrt{3}\cos\theta}\right)^2 \times\left(1-\sin^2\left(\frac{\pi}{3}-\phi\right)\sin^2\theta\right)-\left(\frac{2d_0}{\sqrt{3}}\right)^2 =2s_{11}^M\left(\frac{d_0}{\sqrt{3}}\right)^2+4s_{12}^M\left(\frac{d_0}{\sqrt{3}}\right)^2+2s_{22}^Md_0^2+2s_{33}^Mh_0^2 +4s_{13}^M\frac{1}{\sqrt{3}}d_0h_0+4s_{23}^Md_0h_0, \tag{46}$$

$$\frac{2h_0d_0}{\sqrt{3}}\ \tan\theta(\sqrt{3}\ \sin\phi-\cos\phi)+\left(\frac{2d_0}{\sqrt{3}\ \cos\theta}\right)^2 \times\left[1-\sin^2\left(\frac{2\pi}{3}-\phi\right)\sin^2\theta\right]-\left(\frac{2d_0}{\sqrt{3}}\right)^2 =2s_{11}^M\left(\frac{-d_0}{\sqrt{3}}\right)^2+4s_{12}^M\left(\frac{-d_0}{\sqrt{3}}\right)^2+2s_{22}^Md_0^2+2s_{33}^Mh_0^2 +4s_{13}^M\left(\frac{-d_0h_0}{\sqrt{3}}\right)+4s_{23}^Md_0h_0. \tag{47}$$

Substitution of Eq. (36) into Eqs. (45)–(47) lead to solutions:

$$s_{13}^M=\frac{1}{2}\ \tan\theta\cos\phi,$$

$$s_{23}^M=\frac{1}{2}\ \tan\theta\sin\phi, \tag{48}$$

$$s_{33}^M=0.$$

Regardless of lengthy tedious calculations, the final exact results of s_{ij}^M given by Eqs. (36) and (48) are simple and beautiful. With Eq. (29), the results on s_{ij}^M given by Eq. (48), and the consideration of the C_6 symmetry of the untilt phase, the elastic energy of the L_2 and the L_2' phases is then given by

$$F_e=c_{11}(s_1^2+s_2^2)/2+c_{12}s_1s_2+c_{13}(s_1s_3+s_2s_3) +c_{44}(s_4^2+s_5^2)/2+c_{66}s_6^2/2+c_{33}s_3^2, \tag{49}$$

where the $c_{\mu\nu}$'s are some nonzero components of the elastic constant matrix of hexagonal crystal with $c_{66}=(c_{11}-c_{12})/2$ (see Table 9 of Ref. [19]), and $s_1=s_{11}^M$, $s_2=s_{22}^M$, $s_3=s_{33}^M$, $s_4=2s_{23}^M$, $s_5=2s_{13}^M$, $s_6=2s_{12}^M$. From Eq. (49), the nonzero elements of the stress tensor in the domain system are given by

$$\sigma_{11}^M=\partial F_e/\partial s_1=\tan^2\theta(c_{11}\cos^2\phi+c_{12}\sin^2\phi)/2,$$

$$\sigma_{22}^M=\partial F_e/\partial s_2=\tan^2\theta(c_{11}\sin^2\phi+c_{12}\cos^2\ \phi)/2,$$

$$\sigma_{12}^M=2\partial F_e/\partial s_6=\frac{1}{2}(c_{11}-c_{12})\tan^2\theta\sin2\phi,$$

$$\sigma_{23}^M=2\partial F_e/\partial s_4=2c_{44}\tan\theta\cos\phi,$$

$$\sigma_{13}^M=2\partial F_e/\partial s_5=2c_{44}\tan\theta\sin\phi,$$

$$\sigma_{33}^M=\partial F_e/\partial s_3=\frac{1}{2}c_{13}\tan^2\theta. \tag{50}$$

With the tensor transformation $\sigma_{ij}=R_{ik}R_{jl}\sigma_{kl}^M$ (where $R_{11}=\cos\beta$, $R_{12}=-R_{21}=\sin\beta$, $R_{22}=\cos\beta$, $R_{33}=1$, others are zero, and β is the angle between $\mathbf{x}$ and $\mathbf{x}^M$ [Fig. 1(b)]), the σ_{ij}'s in the laboratory system are given by

$$\sigma_{11,22}=\frac{1}{2}[K\pm\mu(\cos2\phi\cos2\beta+2\sin2\phi\sin2\beta)]\tan^2\theta,$$

$$\sigma_{12}=\sigma_{21}=\frac{1}{2}\mu[2\sin2\phi\cos2\beta-\cos2\phi\sin2\beta]\tan^2\theta,$$

$$\sigma_{13}=2c_{44}\cos(\phi-\beta)\tan\theta,$$

$$\sigma_{23}=2c_{44}\sin(\phi-\beta)\tan\theta,$$

$$\sigma_{33}=\frac{1}{2}C_{13}\tan^2\theta, \tag{51}$$

where $K=(c_{11}+c_{12})/2$, $\mu=(c_{11}-c_{12})/2$ are the plane (hydrostatic) compression modulus and shear modulus, respectively, in a manner as predicted in the classical elasticity theory: The elastic properties of hexagonal crystal are isotropic in the plane perpendicular to the C_6 axis [22]. In other words, the elastic stress is completely determined by the domain orientation (i.e., β), the tilt azimuth ϕ, and the tilt θ (or molecular area A because $A=A_0/\cos\theta$ [2,5,6,23] at L_2 and L_2' phases, where A_0 is the molecular area at untilting phase). Such an apparent expression, Eq. (51), is first obtained, though we note that similar calculation has been carried out in some recent studies by Swanson [34]. If the deformation accompanies a change in the temperature, one has to add a thermal expansion stress tensor $-\alpha_{ij}(T-T_0)$ to σ_{ij}, where the temperature T_0 is defined in the untilting phase (see Ref. [22], p. 14). The complete form of Eq. (23) is then given by

$$t_{ij}^0=-\Pi_{ij}-\alpha_{ij}(T-T_0)-\sigma_{ij}. \tag{52}$$

IV. FLOW-INDUCED ORIENTATION

Now we come to calculate the hydrodynamic stress induced by d_{11} given in Eq. (22). As described in Ref. [23], the results of x-ray diffraction experiments agree with a cylinder tilt packing model (i.e., $\cos\theta = A_0/A$) through L_2 and L_2' phases. Similarly, the 2D flow monolayer as well as the lattice reorientation could be completely determined by the change of molecular tilt and azimuth (i.e., the C_6 axis $\vec{m}$). In other words, the hydrodynamic stress tensor of EL theory [29,30], Eq. (12) is still valid if we consider the C_6 axis $\vec{m}$ as director. Assuming that the NN direction of the discussed domain deviates by an angle β from the x direction then in laboratory system the C_6 axis $\vec{m}$ can be described as [Fig. 1(b)]

$$\vec{m} = (\cos(\phi-\beta)\sin\theta, \sin(\phi-\beta)\sin\theta, \cos\theta), \tag{53}$$

where ϕ is either zero (NN) or $\pi/2$ (NNN) due to the strong coupling between the tilt azimuth and the orientation of the local pseudohexagonal lattice, the effect of lock orientation [1,3,4,8–12]. Both θ and β change with time t represent the orientational effect coming from compression-shear process. Apparently, $\theta(t)$ is given by $\theta = \arccos(A_0/A(t))$ as has been indicated. In addition, with Eqs. (20)–(22), one can have a relation for the shear field θ,

$$\frac{d\theta}{dt} = \dot{\theta} = d_{11}\cot\theta. \tag{54}$$

On the other hand, in previous studies, theoretical study on $\beta(t)$ lacks clear direction [8–12], because its change may be either due to the domain rotation or to the reconstruction of the molecular lattices. In what follows, we try to provide a theoretical treatment for the problem. Firstly, we consider the left side of the 2D Navier-Stokes equation, Eq. (5). With continuity equation, Eq. (17), Eq. (5) may be written as [22]

$$\rho\frac{d\vec{v}}{dt} = \frac{\partial}{\partial t}(\rho\vec{v}) + \vec{\nabla}\cdot(\rho\vec{v}\vec{v}). \tag{55}$$

With Eqs. (18) and (19), together with $X_0(t) = x_0 - v_0 t$ (the position of one barrier), Eq. (55) gives

$$\rho\frac{d\vec{v}}{dt} = 0. \tag{56}$$

In our experiment, $\vec{m}$ is assumed to be homogeneous in domains. Besides, there is no other body forces, i.e., $\vec{f} = 0$. Under these conditions, for our experiment, Eq. (5) leads to

$$\partial_i(t_{ij}' + t_{ij}^0) = 0, \tag{57}$$

a result that satisfies the 2D Navier-Stokes equation. This provides evidence for the prediction given in Sec. I that the CSTAO is described as the dynamical equilibrium between the hydrodynamic stress t_{ij}' and the static stress t_{ij}^0. To further examine the prediction, we first calculate t_{ij}' [Eq. (12)], a general form of tensor combined by the director $\vec{m}$, the flow tensor $\vec{d}$, and the transformed vector $\vec{M}$. The last term $\vec{M}$ defined in Eq. (16), is to replace $d\vec{m}/dt$ as a tensor invariant under proper orthogonal transformation. In the present case of $\vec{w} = 0$, $\vec{M} = d\vec{m}/dt$. Eq. (53) now yields:

$$\vec{M} = \frac{d\vec{m}}{dt} = (\sin(\phi-\beta)\sin\theta, -\cos(\phi-\beta)\sin\theta, 0)\frac{d\beta}{dt} + (\cos(\phi-\beta)\cos\theta, \sin(\phi-\beta)\cos\theta, -\sin\theta)\frac{d\theta}{dt}, \tag{58}$$

where $d\theta/dt$ is given by Eq. (54). In other words, among terms included in t_{ij}', only $\beta(t)$ remains unknown. The dynamical equilibrium equation, Eq. (57), will be used to determine it.

With Eqs. (22), (53), and (58), Eq. (12) gives the apparent expression of t_{ij}' as a function of ϕ, β, θ, and $\dot{\beta}$. Similarly, substitution of Eq. (51) into Eq. (52) yields also an expression of t_{ij}^0 in terms of functions ϕ, β, θ, and $d\beta/dt$. The two calculations are lengthy. The solution of Eq. (57) for $ij = 11, 22$, and 12, respectively, are

$$\begin{aligned}
&[\mu_1\sin^4\theta\cos^4(\phi-\beta) + (\mu_2+\mu_3)\cos^2\theta\cos^2(\phi-\beta) + \mu_4 \\
&\quad + (\mu_5+\mu_6)\sin^2\theta\cos^2(\phi-\beta)]d_{11} \\
&\quad + (\mu_2+\mu_3)\sin^2\theta\cos(\phi-\beta)\sin(\phi-\beta)\frac{d\beta}{dt} + \Pi_{11}^0 \\
&= \Pi_{11} + \alpha_{11}(T-T_0) + \frac{1}{2}\tan^2\theta[K + \mu(\cos 2\phi\cos 2\beta \\
&\quad + 2\sin 2\phi\sin 2\beta)], \quad (i,j=11),
\end{aligned} \tag{59}$$

$$\begin{aligned}
&[\mu_1\sin^4\theta\cos^2(\phi-\beta)\sin^2(\phi-\beta) + (\mu_2+\mu_3) \\
&\quad \times\cos^2\theta\sin^2(\phi-\beta)]d_{11} - (\mu_2+\mu_3)\sin^2\theta\cos(\phi-\beta) \\
&\quad \times\sin(\phi-\beta)\frac{d\beta}{dt} + \Pi_{22}^0 \\
&= \Pi_{22} + \alpha_{22}(T-T_0) + \frac{1}{2}\tan^2\theta[K - \mu(\cos 2\phi\cos 2\beta \\
&\quad + 2\sin 2\phi\sin 2\beta)], \quad (i,j=22),
\end{aligned} \tag{60}$$

$$\begin{aligned}
&[\mu_1\sin^4\theta\cos^3(\phi-\beta)\sin(\phi-\beta) + (\mu_2+\mu_3)\cos^2\theta\sin(\phi \\
&\quad -\beta)\cos(\phi-\beta) + \mu_6\sin^2\theta\cos(\phi-\beta)\sin(\phi-\beta)]d_{11} \\
&\quad + \sin^2\theta[\mu_3\sin^2(\phi-\beta) - \mu_2\cos^2(\phi-\beta)]\frac{d\beta}{dt}
\end{aligned}$$

$$= \frac{1}{2}\mu \tan^2\theta[2\cos 2\beta \sin 2\phi - \sin 2\beta \cos 2\phi],$$

$$(ij = 12). \tag{61}$$

Π_{11}^0 and Π_{22}^0 are integral constants, their physical meaning will be given later. Here, in the derivation of Eq. (61), taking account of the geometry of our experiment, we have invoked $\Pi_{12} = 0$. This assumption implies that; due to symmetry, the domain orientation will be either parallel or perpendicular to the flow direction. Such consideration was also invoked by Fuller's group, e.g., they argued that "because of the symmetry of the four-roll mill flow, any flow-induced orientations must appear at 0° or 90° relative to the flow direction" [9]. The main progress of the present theory is the description of how the orientation can occur. For domains of L_2 phase where $\vec{m}$ tilts along the NN direction (i.e., $\phi = 0$), with some algebraic transformation, the above three equations together with Eq. (22) yield

$$\Pi = \Pi^0 - \alpha(T - T_0) - \frac{1}{2}K \tan^2\theta - \frac{V_{AC}}{2A_0}\cos\theta[\mu_1 \sin^4\theta\cos^2\beta + (\mu_2 + \mu_3)\cos^2\theta + \mu_4 + (\mu_5 + \mu_6)\sin^2\theta\cos^2\beta], \tag{62}$$

$$\Delta\Pi = \Delta\Pi^0 - \Delta\alpha(T - T_0) - \mu \tan^2\theta\cos 2\beta - (\mu_2 + \mu_3)\sin^2\theta \sin 2\beta \frac{d\beta}{dt}$$
$$- \frac{V_{AC}}{A_0}\cos\theta[\{\mu_1 \sin^4\theta\cos^2\beta + (\mu_2 + \mu_3)\cos^2\theta\}\cos 2\beta + \mu_4 + (\mu_5 + \mu_6)\sin^2\theta\cos^2\beta], \tag{63}$$

$$\frac{d\beta}{dt} = \frac{\left[\mu \tan^2\theta + \left(\frac{V_{AC}\cos\theta}{A_0}\right)\{\mu_1 \sin^4\theta\cos^2\beta + (\mu_2 + \mu_3)\cos^2\theta + \mu_6 \sin^2\theta\}\right]\sin 2\beta}{[(\mu_2 - \mu_3) + (\mu_2 + \mu_3)\cos 2\beta]\sin^2\theta}, \tag{64}$$

where $\Pi = (\Pi_{11} + \Pi_{22})/2$, $\Delta\Pi = \Pi_{11} - \Pi_{22}$ are the isotropic part and the anisotropic part of Π_{ij}. These for $\Pi^0 = \frac{1}{2}(\Pi_{11}^0 + \Pi_{22}^0)$, $\alpha = \frac{1}{2}(\alpha_{11} + \alpha_{22})$, $\Delta\alpha = \alpha_{11} - \alpha_{22}$. As $V_{AC} \to 0$, $\theta \to 0$, Eqs. (62) and (63) lead to $\Pi = \Pi^0$ and $\Delta\Pi = \Delta\Pi^0$, i.e., Π^0 and $\Delta\Pi^0$ are the isotropic and the anisotropic parts of Π_{ij} at the equilibrium untilting phase, i.e., the S phase. In Ref. [4], the observation by x-ray diffraction experiment, $\Delta\Pi^0$ is also nonzero since in the $L_2' \to S$ transition the tilt angle tends to become zero, but the head groups remain arranged on the distorted hexagonal lattice. From Eqs. (62) and (63), one finds that Π, α, K appear in one equation and $\Delta\Pi, \Delta\alpha, \mu$ in another. This comes from the fact that members of each group have the same symmetry. This can be used as a check for the above derivation. It is interesting to note that $\Delta\Pi$-$\Delta\Pi^0$ and Π-Π^0 do not vanish even in the untilted phase ($\theta = 0$) on account of the contribution of compression shear $V_{AC} \neq 0$. In physics, this is true, because $V_{AC} \neq 0$ means the monolayers are not in real isothermal transition. Equation (64) shows the most important conclusion, that is, $\beta \to 0$, π or $\pm\pi/2$ are two possible stable states on account of $d\beta/dt = 0$ in both cases. This confirms the finding by Fuller's group [8–12]: the domain tilt will orient either along or against the flow direction, or normal to the flow direction. Moreover, Eq. (64) can be rewritten as

$$\frac{d\sin^2\beta}{dt} = \frac{\left[\mu \tan^2\theta + \left(\frac{V_{AC}\cos\theta}{A_0}\right)\{\mu_1 \sin^4\theta\cos^2\beta + (\mu_2 + \mu_3)\cos^2\theta + \mu_6 \sin^2\theta\}\right]\sin^2 2\beta}{[(\mu_2 - \mu_3) + (\mu_2 + \mu_3)\cos 2\beta\sin^2\theta}. \tag{65}$$

Generally, we have $\mu_1 \sin^4\theta\cos^2\beta + (\mu_2 + \mu_3)\cos^2\theta + \mu_6 \sin^2\theta < 0$ and $(\mu_2 - \mu_3) + (\mu_2 + \mu_3)\cos 2\beta < 0$ are held [for N-(p-methoxybenzylidene)-p′-buthylaniline (MBBA), $\mu_2 = -77.5$, $\mu_3 = -1.2$, $\mu_1 = 6.5$, $\mu_6 = -34.4$ CP [36]]. From Eq. (65), we find that the interesting result that there exists a threshold of compression shear

$$V_{AC}^*(NN) = \frac{-A_0\mu\sin^2\theta}{\cos^3\theta[\mu_1 \sin^4\theta\cos^2\beta + (\mu_2 + \mu_3)\cos^2\theta + \mu_6 \sin^2\theta]} > 0. \tag{66}$$

Below the threshold $[V_{AC}<V_{AC}^{*}(\mathrm{NN})]$, one finds that $d\sin^2\beta/dt<0$, i.e., β is monotonously decreasing to 0 or increasing to π. This means that the flow-induced orientation starts from the very small compression shear in the L_2 phase. Therefore, on account of $\gamma=\beta$, a steady compression can induce nonvanishing $\langle\cos^3\gamma\rangle$ and $\langle\cos\gamma\rangle$ in Eq. (3). This prediction is well confirmed by our SHG measurement in the 7OCB monolayer. We detected an increasing $I_{s\text{-}s}$ SHG signal as the molecular area begins to become less than 42 Å^2, i.e., the appearance of a L_2 phase transition. The I_{s-s} curve given on the top of Fig. 3 shows nonmonotonous increase with the compression. This is also in good agreement with the theoretical prediction. In Eq. (3), the formula of $P_{s\text{-}s}^{N}$, the terms $\langle\cos\gamma\rangle$ and $\langle\cos^3\gamma\rangle$ increase with the flow-induced orientation, however, the coefficients $\sin\theta$ and $\sin^3\theta$ decrease with the compression, respectively. The flow behavior in L_2 phase can be discussed qualitatively by the above analysis. Equation (63) indicates clearly that the L_2 phase tension shows anisotropy. This has been reported in the experiment of uniaxially compressed heneicosanoic acid monolayer [37]. More anomalous properties of surface tension Π and its anisotropy $\Delta\Pi$ given in Eqs. (62) and (63) show dependence on the compression shear V_{AC} and the flow-induced orientation [relating to $\beta(t)$]. For discussion on Eq. (66), the flow orientation is always easy to be achieved. Therefore, for a spatially steady flow field, once the orientation is established (i.e., $\beta=0$ or π), both Π and $\Delta\Pi$ do not depend on the stochastic factor of $\beta(t)$ and the shape deformation of the domains induced by Π and $\Delta\Pi$ with change of V_{AC} is affined and reversible. This explains qualitatively the observation reported by Fuller's group [8–12]. Despite of the fact that the fluid fields of our simple compression are different from those generated by the four-roll mill (see, e.g., Fig. 2 in Ref. [9]), the flows of the latter at the ''shear bands'' with $\pm45°$ to x and y axes are nearly the same as ours. Therefore, the above analysis satisfies qualitatively in these regions, where the domain distortion of L_2 phase was found to be reversible, and the initial domain pattern could be approximately restored during a reversal of the flow direction (Fig. 4 in Ref. [9]). The behavior of the L_2' phase will be shown to be different from that of L_2 phase. Putting $\phi=\pi/2$ [i.e., NNN tilt, Fig. 1(b)], the calculation similar to the derivation of Eqs. (62)–(64) gives the following relations:

$$\Pi=\Pi^0-\alpha(T-T_0)-\frac{1}{2}K\tan^2\theta-\frac{V_{AC}}{2A_0}\cos\theta\times[\mu_1\sin^4\theta\sin^2\beta+(\mu_2+\mu_3)\cos^2\theta+\mu_4+(\mu_5+\mu_6)\sin^2\theta\sin^2\beta], \tag{67}$$

$$\Delta\Pi=\Delta\Pi^0-\Delta\alpha(T-T_0)+\mu\tan^2\theta\cos2\beta+(\mu_2+\mu_3)\sin^2\theta\sin2\beta\frac{d\beta}{dt}+\frac{V_{AC}}{A_0}\times\cos\theta[\{\mu_1\sin^4\theta\cos^2\beta+(\mu_2+\mu_3)\cos^2\theta\}\times\cos2\beta-\mu_4-(\mu_5+\mu_6)\sin^2\theta\sin^2\beta], \tag{68}$$

$$\frac{d\beta}{dt}=\frac{\left[\mu\tan^2\theta+\left(\frac{V_{AC}\cos\theta}{A_0}\right)\{\mu_1\sin^4\theta\sin^2\beta+(\mu_2+\mu_3)\cos^2\theta+\mu_6\sin^2\theta\}\right]\sin2\beta}{[(\mu_3-\mu_2)+(\mu_2+\mu_3)\cos2\beta]\sin^2\theta}. \tag{69}$$

They are the same equations Eq. (62), Eq. (63), and Eq. (64), respectively. Equation (69) can also be written as

$$\frac{d\sin^2\beta}{dt}=\frac{\left[\mu\tan^2\theta+\left(\frac{V_{AC}\cos\theta}{A_0}\right)\{\mu_1\sin^4\theta\sin^2\beta+(\mu_2+\mu_3)\cos^2\theta+\mu_6\sin^2\theta\}\right]\sin^2 2\beta}{[(\mu_3-\mu_2)+(\mu_2+\mu_3)\cos2\beta]\sin^2\theta}. \tag{70}$$

With the same estimate for μ_1, μ_2, μ_3, and μ_6 as above, we find that under the similar orientation condition, there exists a threshold

$$V_{AC}^{*}(\mathrm{NNN})=\frac{-A_0\mu\sin^2\theta}{\cos^3\theta[\mu_1\sin^4\theta\sin^2\beta+(\mu_2+\mu_3)\cos^2\theta+\mu_6\sin^2\theta]}. \tag{71}$$

Below the threshold, $d\sin^2\beta/dt>0$ is always true, i.e., β is monotonously decreasing to $-\pi/2$ or increasing to $\pi/2$, corresponding to tilt along the flow or against the flow, respectively [see Fig. 1(b)]. There is no difference of the flow-induced orientation at low V_{AC}. Especially, the substitution of $\beta=0,\pi$ into Eq. (66) and $\beta=\pm\pi/2$ into Eq. (71), gives the expressions

$$V_{AC}^{*}(\mathrm{NN})=\frac{-A_0\mu\sin^2\theta}{\cos^3\theta[(\mu_1\sin^2\theta+\mu_6)\sin^2\theta+(\mu_2+\mu_3)\cos^2\theta}, \tag{72}$$

and

$$V_{AC}^{*}(\mathrm{NNN})=\frac{-A_0\mu\sin^2\theta}{\cos^3\theta[(\mu_1\sin^2\theta+\mu_6)\sin^2\theta+(\mu_2+\mu_3)\cos^2\theta}. \tag{73}$$

However, it is the expressions L_2(NN) and L_2'(NNN) phase reveal the difference of the flow behavior. L_2 happens at low surface pressure, while L_2' at high surface pressure [8–12]. The fact that θ^{NN} is always larger than θ^{NNN} leads to

$$V_{AC}^{*}(\mathrm{NNN})<V_{AC}^{*}(\mathrm{NN}). \tag{74}$$

In other words, the equilibrium of the orientation along or against the flow is broken easier in L_2' than in L_2, i.e., as $V_{AC}>V_{AC}^{*}$, the tilt will change to be normal to the flow. This may give an interpretation of the finding by Fuller's group that L_2' shows more obvious flow induced reorientation than L_2 [10]. In fact, as mentioned earlier, they found the same result as ours that extensional flows of sufficient magnitude can induce the tilt azimuth to align perpendicular to the extensional axis for molecules at the ''shear bands,'' where the hexatic lattice undergoes homogeneous shear. The tilt of L_2' normal to the flow is also reported by the same group [8–10]. This may happen in the case of $V_{AC}^{*}(\mathrm{NNN})<V_{AC}<V_{AC}^{*}(\mathrm{NN})$. The tilt orientation changes from parallel to the flow to normal to the flow at $V_{AC}=V_{AC}^{*}$, and will cause a sudden change of $d\beta/dt$ and so for $\Delta\Pi$ [see, Eq. (68)]. The latter will induce a strong nonsymmetric deformation of the domain and even a breakup of the domains as was observed by Fuller's group [10].

The shear-induced molecular precession in L_2' discovered by Ignes-Mullol and Schwartz [11] is the case that the shear flow induces not only domain rotation but also cooperative continuum rotation of the molecular orientation. In order to treat this situation the above ϕ-lock assumption of letting $\phi=0$ or $\pi/2$ must be changed to $\phi=\phi(t)$. This is possible in some higher temperature phases such as O_v phase, where the molecular tails have more activity. The calculation with the present model for this case is in progress and will be reported in the future. In principle, it is not difficult in understanding the present model.

It is interesting to compare the present model with previous theoretical work on static elastic models in 2D systems. In the work of generalized Wulff construction to 2D materials of orientational order but without positional order, Rudnick and Bruinsma have argued that the 2D anisotropic surface energy $\sigma(\beta)=\sigma_0+a_2\cos 2\beta$ corresponds to 2D nematic [38]. Our present result shown in Eqs. (62), (63), (67), and (68) gives a similar expression for the surface stress tensor (our Π, $\Delta\Pi$ have the same meaning as σ in Ref. [38]) that the monolayer of L_2 and L_2' phases can be treated as 2D nematic LC but their σ_0 and a_2 will vary with the tilt angle θ and the flow fields. In a very recent study on the analysis of the flow-induced domain formation in L_2', the so-called ''shear bends'' reported in Ref. [9] we also showed that the 2D surface stress tensor has to include the hydrodynamic (i.e., viscous) component given in Eq. (12) [39]. These features are different from those described in Ref. [38].

Finally, for future use, we should note that the elastic moduli K, μ, and the EL's viscosity coefficients $\mu_1-\mu_6$ appeared above are defined in the 2D system, therefore, their values can be estimated by the corresponding values in the 3D system divided by h_0 for K, and μ and multiplied by h_0 for $\mu_1-\mu_6$. Here, h_0 is the length of the molecular tail in monolayers. Such a simple scaling treatment is based on the feature that a monolayer can be seen as a 3D layer with thickness of h_0. The 2D K, μ of crystalline decanol monolayer have been measured by x-ray diffraction by Zakri *et al.* [24] but with some uncertainty [25]. The 2D values of $\mu_1-\mu_6$ of monolayer have not been reported in literature, however, we can use 3D values of μ_{1-6}^{3D} in LC (about 10^{-2}–10^{-1} g/cm s [14], p. 150) to estimate 2D μ_{1-6} as $\mu_{1-6}^{3D}\cdot h_0\sim 10^{-6}$–$10^{-5}$ g/s with $h_0\sim 10^{-4}$ cm. The result is in precise agreement with the typical surface viscosity measured by Schwartz and his co-workers [12] in channel flow in a Langmuir monolayer and a calculation by Stone in a theoretical analysis [26]. This gives evidence for the present theory. With above estimate for μ_{1-6}, $A_0\approx 20$ Å^2, and the lower value of $\mu=1$ mN/m measured by Zakri and Berge [25], we obtain from Eq. (71), $V_{AC}^{*}(\mathrm{NNN})\approx 2\times 10^6\sin^2\theta$ Å$^2/s=1.2\times 10^8\sin^2\theta$ Å^2/min. In other words, $V_{AC}=5.6$ Å^2/min in our MDC-SHG experiment discussed in Sec. II is far away to achieve V_{AC}^{*} except for $\theta<0.01°$. Therefore, on the way from NNN$\rightarrow U$ phase transition, we cannot find a distinguishable reorientation in our experiment. This is again true as shown in Fig. 3. The above estimation is still a rough approximation because we have used the data of μ_{1-6}^{3D} obtained from bulk MBBA and p-azoxyanisole (PAA). They are rather rigid LC molecules and do not have much in common with fatty acids in Fuller's experiments. Therefore, a measurement of V_{AC}^{*} on the fatty acids to provide more exact values of their μ_{1-6}^{2D} is a challenge in future study.

V. CONCLUSION

We have treated the flow-induced tilt azimuth orientation of monolayers in L_2 and L_2' phases as dynamical equilibrium

between viscous and elastic stresses by successfully adapting the Leslie-Ericksen theory for liquid crystal dynamics. The BAM-observed facts in the flow-induced orientation of Langmuir monolayers in condensed phases [8–12] as well as the MDC-SHG observation of $P^N_{s-s} \neq 0$ in the 7OCB monolayers obtained here do confirm our theoretical prediction. In other words, the present study establishes an accepted model for the hexatic flow.

[1] G.L. Gaines, *Insoluble Monolayers at the Liquid-Gas Interfaces* (Interscience, New York, 1966).

[2] V.M. Kaganer, H. Möhwald, and P. Dutta, Rev. Mod. Phys. **71**, 779 (1999).

[3] D.R. Nelson and B.I. Halperin, Phys. Rev. B **21**, 5312 (1980).

[4] P. Dutta, J.B. Peng, B. Lin, J.B. Ketterson, M. Prakash, P. Georgopoulos, and S. Ehrlich, Phys. Rev. Lett. **58**, 2228 (1987); K. Kjaer, J. Als-Nielsen, C.A. Helm, L.A. Laxhuber, and H. Mohwald, *ibid.* **58**, 2224 (1987).

[5] M. Iwamoto and Z.C. Ou-Yang, J. Chem. Phys. **117**, 7705 (2002).

[6] M. Iwamoto, T. Manaka, A. Tojima, and Z.C. Ou-Yang, Chem. Phys. Lett. **355**, 169 (2002).

[7] I.R. Peterson, V. Brzezinski, R.M. Kenn, and R. Steitz, Langmuir **8**, 2995 (1992).

[8] M.C. Friedenberg, G.B. Fuller, C.W. Frank, and C.R. Robertson, Langmuir **12**, 1594 (1996).

[9] T. Maruyama, G.B. Fuller, C.W. Frank, and C.R. Robertson, Science **274**, 233 (1996).

[10] T. Maruyama, J. Lauger, G.G. Fuller, C.W. Frank, and C.R. Robertson, Langmuir **14**, 1836 (1998).

[11] J. Ignés-Mullol and D.K. Schwartz, Phys. Rev. Lett. **85**, 1476 (2000).

[12] D.K. Schwartz, C.M. Konbler, and R. Bruinsma, Phys. Rev. Lett. **73**, 2841 (1994).

[13] W. Helfrich, J. Chem. Phys. **50**, 100 (1969).

[14] S. Chandrasekhar, *Liquid Crystals*, 2nd ed. (Cambridge University Press, Cambridge, 1992), p. 97.

[15] M. Iwamoto, Y. Majima, H. Naruse, T. Noguchi, and H. Fuwa, Nature (London) **353**, 645 (1991).

[16] M. Iwamoto, C.X. Wu, and Z.C. Ou-Yang, Chem. Phys. Lett. **325**, 545 (2000).

[17] A. Tojima, Y. Matsuo, R. Hiyoshi, T. Manaka, Y. Majima and M. Iwamoto, Thin Solid Films **393**, 86 (2001).

[18] A. Tojima, T. Manaka, and M. Iwamoto, J. Chem. Phys. **115**, 9010 (2001).

[19] J.F. Nye, *Physical Properties of Crystals* (Oxford University Press, Oxford, 1957).

[20] For a review, see examples, D. A. Edwards, H. Brenner, and D. T. Wasan, *Interfacial Transport Processes and Rheology* (Butterworth-Heinemann, Boston, 1991).

[21] W.D. Harkins and J.G. Kirkwood, J. Chem. Phys. **6**, 53 (1938).

[22] L.D. Landau and E. M. Lifshiz, *Theory of Elasticity*, 3rd ed. (Pergamon, Oxford, 1959), pp. 10, 35.

[23] K. Kjaer, J. Als-Nielsen, C.A. Helm, P. Tippman-Krayer, and H. Moehwald, J. Phys. Chem. **93**, 3200 (1989).

[24] C. Zakri, A. Renault, J. Rieu, M. Vallade, B. Berge, J. Legrand, G. Vignault, and G. Grubel, Phys. Rev. B **55**, 14 163 (1997).

[25] C. Zakri and B. Berge, Physica B **248**, 208 (1998).

[26] H.A. Stone, Phys. Fluids **7**, 2931 (1995).

[27] H.A. Stone and H.M. McConnel, Proc. R. Soc. London, Ser. A **448**, 97 (1994).

[28] R.E. Goldstein and D.P. Jackson, J. Phys. Chem. **98**, 9626 (1994).

[29] J.L. Ericksen, Arch. Ration. Mech. Anal. **4**, 231 (1964); Trans. Soc. Rheol. **5**, 123 (1961).

[30] F.M. Leslie, Q. J. Mech. Appl. Math. **19**, 357 (1966); Arch. Ration. Mech. Anal. **28**, 265 (1968).

[31] C.W. Oseen, Trans. Faraday Soc. **29**, 883 (1933); H. Zocher, *ibid.* **29**, 945 (1933); F.C. Frank, Discuss. Faraday Soc. **25**, 19 (1958).

[32] Z.C. Ou-Yang and L. Ji-xing, Phys. Rev. Lett. **65**, 1679 (1990); Phys. Rev. A **43**, 6826 (1991).

[33] S. Komura and Z.C. Ou-Yang, Phys. Rev. Lett. **81**, 473 (1998).

[34] D.R. Swanson, T. Luty, and C.J. Eckhardt, J. Chem. Phys. **107**, 4744 (1997); T. Luty, D.R. Swanson, and C.J. Eckhardt, *ibid.* **110**, 2606 (1999); T. Luty, C.J. Eckhardt, and J. Lefebvre, *ibid.* **111**, 10321 (1999); C. Fradin, J. Daillant, A. Braslau, D. Luzet, M. Alba, and M. Goldmann, Eur. Phys. J. B **1**, 57 (1998).

[35] E.B. Sirota, Langmuir **13**, 3849 (1997).

[36] P.G. de Gennes and J. Prost, *The Physics of Liquid Crystals*, (Clarendon Press, Oxford, 1993), p. 231, Table 5.1, The values and signs of $\mu_1 - \mu_6$ for PAA LC is similar to the case of MBBA (see, p. 150, Ref. [13]).

[37] T.M. Bohanon, A.M. Lee, J.B. Ketterson, and P. Dutta, Langmuir **8**, 2479 (1992).

[38] J. Rudnick and R. Bruinsma, Phys. Rev. Lett. **74**, 2491 (1995).

[39] M. Iwamoto and Ou-Yang Zhong-can (unpublished).

[40] A. Tojima *et al.*, in *Book of Abstracts*, The 19th International LC Conference, 2002, Edinburgh, United Kingdom (Royal Society of Chemistry, London, 2002), p. 336.